# Improving cellular migration in tissue engineered laryngeal scaffolds

**[1]Kurt Wismayer, [2]Nazia Mehrban, [3]James Bowen, [4]Martin Birchall**

[1] Dr. Kurt Wismayer MD, MSc (UCL)
kurtwism1989@gmail.com
Division of Surgery, University College London, London, WC1E 6BT, United Kingdom.
[2] Dr. Nazia Mehrban PhD
n.mehrban@ucl.ac.uk
Division of Surgery, University College London, London, WC1E 6BT, United Kingdom.
[3] Dr. James Bowen PhD, MEng
james.bowen@open.ac.uk
The Open University, School of Engineering and Innovation, Milton Keynes, MK7 6BJ, United Kingdom.
[4] Prof Martin Birchall MA (Hons), MD (Cantab.), FRCS, F.Med.Sci
m.birchall@ucl.ac.uk
Ear Institute, University College London, London, WC1X 8DA, United Kingdom.

**Corresponding Author**
Name: Dr. Kurt Wismayer
Address: Doctor's Office, 10 South Ward, Charing Cross Hospital, Fulham Palace Road, London W6 8RF, United Kingdom.
Contact Number: +44 (0)7598432544
E-mail: kurtwism1989@gmail.com

**Footnotes**
Presented at the Association of Surgeons in Training 2017 conference, 31st March – 2nd April, 2017, Bournemouth, United Kingdom.

**Abstract**
To modify the non-porous surface membrane of a tissue-engineering laryngeal scaffold to allow effective cell entry.

The mechanical properties, surface topography and chemistry of polyhedral oligomeric silsesquioxane polymer poly(carbonate-urea) urethane (POSS-PCU) were characterised. A laser technique introduced surface perforations. Micro computed tomography (microCT) generated porosity data. Scaffolds were seeded with cells, investigated histologically and proliferation studied. Incubation and time effects were assessed.

Laser-cutting perforated the polymer, connecting the substructure with the ex-scaffold environment and increasing porosity (Porous, Non-perforated: 87.9%, Porous, laser-perforated at intensities 3: 96.4% and 6: 89.5%). Cellular studies confirmed improved cell viability. Histology showed cells adherent to the scaffold surface, cells within perforations and indicated that cells migrated into the scaffolds. After 15 days of incubation, scanning electron microscopy revealed an 11% reduction in pore diameter, correlating with a decrease in Young's Modulus.

Introducing surface perforations presents a viable method of improving POSS-PCU as a tissue-engineering scaffold.

**Key Words**
Tissue Engineering, Laryngeal Neoplasms, Porosity, Cell proliferation, POSS-PCU polymer, Tissue Scaffolds.

**Abbreviations**

ANOVA – Analysis of Variance
DMAC – Dimethylacetamide
DMEM – Dulbecco's Modified Eagle's Medium
EHT – Extra-High Tension
FBS – Foetal Bovine Serum
H&E – Haematoxylin and Eosin
MDI – Methylenebis(phenyl isocyanate)
MF – Murine Fibroblasts
MPa – Megapascal
$NaHCO_3$ – Sodium Bicarbonate
NBF – Neutral Buffered Formalin
PBS – Phosphate-Buffered Saline
PEC – Porcine Epithelial Cells
PF – Porcine Fibroblasts
PL – Partial Laryngectomy
POSS-PCU – Polyhedral Oligomeric Silsesquioxane Poly(Carbonate-Urea) Urethane
ROCK – Rho-associated coiled coil forming protein serine/threonine kinase
RPM – Revolutions per Minute
SEM – Scanning Electron Microscope
TE – Tissue Engineering
TL – Total Laryngectomy

## 1. Introduction

The management of advanced laryngeal cancer (about 2000 cases per annum UK[1]) often involve partial (PL) or total laryngectomy (TL), which carry significant mortality (0.5% [2]) and morbidity (20-40% [3]). For the majority of survivors, altered voice, swallowing and breathing, activity, appearance, smell and taste, amongst other problems, cause a considerable reduction in quality of life [4, 5].

Tissue engineered (TE) airway scaffolds have now been successfully used in compassionate settings [6-8], raising the possibility that this technology may be extended to laryngeal reconstruction [9]. Such successes have instigated a search for the ideal material for implantable scaffolds [10], based on both natural and synthetic materials [11].

There are significant challenges to controlling and quality controlling the chemical and physical properties, and behaviour *in vivo*, of biological raw materials such as laminin and collagen [12]. Synthetic materials such as poly(urethane) and biodegradable glass, being comparatively easy to manufacture, offer relatively unrestricted availability, as well as the potential to modify their properties to suit purpose [13], particularly pertinent to demanding clinical applications such as airway replacement.

A polymer's mechanical properties and pre-disposition to cellular attachment can be significantly altered by the addition of specific molecules [14, 15]. One such nano-composite is polyhedral oligomeric silsesquioxane poly(carbonate-urea) urethane (POSS-PCU). This non-biodegradable family of polymers has been shown to possess *in vivo* biostability*, effective mechanical strength, as well as biocompatibility [16].

* *In vivo* biostability is described by Anderson & Zhao, 2013 (Anderson, J., & Zhao, Q. (1991). Biostability of Biomedical Polymers. MRS Bulletin, 16(9), 75-77. doi:10.1557/S0883769400056098; https://www.cambridge.org/core/journals/mrs-bulletin/article/biostability-of-biomedical-polymers/0FC3680E735F04BE8E92A71F70A83D7F), as a term which 'commonly refers to the relative stability of biomedical polymers in the physiological environment as a function of time.'

Tissue-engineered scaffolds of hollow viscera should maintain barrier function whilst supporting tissue and vascular regeneration [17, 18]. Although POSS-PCU's semi-closed pore architecture supports its surface integrity, gaining access to the porous inner structure has been an issue. The addition of porogens (pore-forming solid particles) during POSS-PCU synthesis improves its internal porosity. However, unpublished preliminary work from our group shows that this is counteracted by the formation of a 'skin' on the polymer's surface occurring on contact with deionised water during the solidification process. Here, we investigated methods to modify POSS-PCU surface permeability whilst using porogen to increase internal porosity. We studied resultant changes in surface topography, mechanical and chemical properties, porosity and biocompatibility. The effect of time and incubation on treated and untreated scaffolds was also investigated. We hypothesised that perforating the impermeable surface of POSS-PCU would lead to improved cellular migration into the scaffold.

## 2. Materials and Methods

For the purposes of this study incubation was always carried out at 37ºC, 5% $CO_2$ and 100% relative humidity.

### 2.1 POSS-PCU Synthesis

POSS-PCU was synthesised using a previously reported method [19]. Briefly, trans-cyclohexanechloroydrinisobutyl-silsesquioxane and polycarbonate polyol were added to a reaction flask fitted with a mechanical stirrer and nitrogen inlet. This mixture was then heated to 135°C allowing the POSS cage to dissolve in the polyol and then cooled to 70°C. Flake 4,4'-methylenebis(phenyl isocyanate) (MDI) was added to the mixture and reacted (under nitrogen and at 75°C - 85°C) for 90 minutes forming a pre-polymer. Dimethylacetamide (DMAC) was slowly added to the pre-polymer and the resultant solution was cooled to 40°C. Ethylenediamine, dissolved in DMAC, was then added, drop wise, to the mixture for chain extension of the pre-polymer to occur, resulting in the formation of a POSS modified polycarbonate urea-urethane solution, dissolved in DMAC.

### 2.2 Porous POSS-PCU Fabrication

Porogen (refined grade sodium bicarbonate ($NaHCO_3$; Tata Chemicals Europe, UK); sieved, using stainless steel sieves (Fisher Scientific, Leicestershire, UK), to a 53-100µm average granule size) was added to 18 wt% POSS-PCU and TWEEN® 20 (Sigma-Aldrich Ltd, UK) surfactant (20% $NaHCO_3$ : 78% POSS-PCU : 2% TWEEN® 20; w/w/w) to form the test foam elastomer polymer sheets via porogen leaching and coagulation methods [20]. Control polymer sheets were formed similarly, without porogen being added. Briefly, the polymer was mixed using a Thinky AER 250 mixer (Intertonics, UK), at 3000rpm for 3 minutes, then poured onto glass plates with a 300 µm thick wall around the edges. The mixture was spread using a rod to ensure an even coating. The plates were then submerged in deionised water and left to coagulate for 3 days, with the water being changed 3 times per day. The polymer sheets were then removed from the glass plates and stored under deionised water, at room temperature.

### 2.3 Perforation of POSS-PCU

Two techniques were devised to perforate the surface of porous and non-porous samples.

#### 2.3.1 Laser Technique

A laser cutter (Intensity (P) 6, Velocity (V) 0.60 Pulses (PPI) 1000; Speedy300™, Trotec®, US) was used to cut a polymer disc and perforate it at randomly-selected, incremental distances of 0.31mm, 0.49mm, 0.67mm, 0.89mm, 1.08mm and 1.4mm. The disc was then imaged via scanning electron microscopy (SEM) to select an inter-perforation distance, which avoided overlapping or abutting of perforations. The optimal distance selected was of 1.4mm. Various laser intensities were then appraised and two selected; 3 and 6. Sheets were laser-perforated, cut into appropriate shapes and stored under sterile phosphate-buffered saline (PBS).

#### 2.3.2 Mechanical Method

Custom-made equipment was set up (Figure 1) with a spiked titanium roller, acting at two forces. The stiffness, or spring constant, of the compliant element of the apparatus (Kit No.251, Lee Spring UK) was measured using an Instron 5565 tester (500 N Load Cell; Instron Ltd, Bucks, UK).

Squares (53mm x 53mm) were cut from porous and non-porous sheets of polymer using a laser-cutter (Speedy300™, Trotec®, US), placed in the petri dish and the platform raised until the spikes of the microneedle roller (540 Titanium Micro Needles Derma Microneedle Roller 2.5mm; Sodacoda Ltd., UK) just touched the polymer. This was then raised a further distance to be perforated at the required force. The drawer was then pulled out at a steady pace such that the spiked roller ran over the entire polymer surface. These sheets were cut into dumbbells (in accordance with ISO 37 specifications) for tensile testing, discs cut for cellular experiments, and off-cuts used for scanning electron microscopy imaging.

#### 2.3.3 Sample Codes

Initially, 2 batches of POSS-PCU were used in polymer fabrication – Sample 1 and Sample 2. Sample 2 POSS-PCU was synthesised 6 months after Sample 1. The forces to be used for mechanical perforation were initially arbitrarily chosen as 2.5N and 5.0N. The

changes in platform height associated with these forces were derived. In practice, the closest forces to these values achievable using this method were 2.6N and 5.2N and these were therefore used throughout this study.

**2.4 Surface Wetness using Contact Angle Measurement**

Drop-shape analysis was used to determine the material's hydrophilicity/hydrophobicity. The Sessile Drop method was used to measure the contact angle between a droplet of deionised water and the POSS-PCU surface and analysis of this was carried out via a KRÜSS DSA 100, Drop Shape Analyser (KRÜSS GmbH, Germany).

Contact angle measurements of non-porous and porous samples were compared. Contact angle readings of porous samples 6 months post-synthesis were measured in order to assess potential changes with time.

**2.5 Mechanical Properties**

Specimens were first cut into dumbbells (in accordance with ISO 37 specifications) using a laser-cutter (Intensity (P) 6, Velocity (V) 0.60 Pulses (PPI) 1000; Speedy300™, Trotec®, US) and their tensile properties were assessed using an Instron 5565 tester (500 N Load Cell; separation distance 20 mm; Instron Ltd, Bucks, UK), after the thickness of each dumbbell was assessed and noted using digital callipers . The relationship between stress and strain was analysed as per ISO 37 and the rate of displacement was set at 50mm $min^{-1}$. Bluehill software was used to calculate Young's Modulus from the linear region of the plot within 0-5mm displacement. Briefly, stress, strain and Young's Modulus were calculated using Equations 2-4 [21]:

$$E = \sigma / \varepsilon \quad (1)$$

where E is the Young's Modulus ($N/m^2$) of the material under investigation, σ is the normal stress ($N/m^2$) and ε is a unit-less measure of engineering strain applied to the material under investigation. The two components of this equation required to calculate E, σ and ε, can be calculated using the equations:

$$\sigma = F_n / A \quad (2)$$

where σ is the normal stress ($N/m^2$) applied across the area of the material under investigation, $F_n$ is the normal component force (N) applied to this area, and A is the area ($m^2$) of the material itself. And:

$$\varepsilon = dl / l_0 \quad (3)$$

where ε is a unit-less measure of the engineering strain applied to the material under investigation, dl is the change of length (m) and lo = initial length (m) of the material under investigation.

Tensile testing was also used to compare the mechanical properties of porous, unperforated samples synthesised 6 months apart in order to assess the effect of time.

The effect of time and incubation on the mechanical properties of treated, porous POSS-PCU was also assessed. Briefly, polymer dumbbells cut and laser/mechanically-treated on day 0, were tensile tested. They were then stored in sterile PBS, changed 3 times weekly and incubated to simulate conditions to be used in cellular studies. Tensile testing was repeated on day 15.

**2.6 Imaging**

Samples were dehydrated by serial submersion in 100% ethanol for 15 minutes and then dried by either critical point drying (CPD; Balzers® model CPD 020, Balzers AG, Principality of Liechtenstein) over 3 hours or freeze dried using a Labconco freeze dryer (model 4.5, Labconco Corp., US) with a temperature setting of -50°C and a vacuum of less than 10μm of Hg for 4 hours.

**2.6.1 Scanning Electron Microscopy**

Samples were dried via CPD and then coated with gold (film thickness 20nm) using a rotary-pumped sputter coater (Q150R, Quorum Technologies Ltd, UK). An SEM (EVO-HD15, Carl Zeiss GA, Germany) was used to image volar, dorsal and cross-sectional aspects of samples at various magnifications.

Samples imaged on day 0 of perforation were first dried via CPD and then coated with gold/palladium (fil thickness 2-3nm) using an ion beam coater (Model 681, Gatan inc., US). Samples imaged on day 15 were freeze dried and then coated with gold using a rotary-pumped sputter coater (Q150R, Quorum Technologies Ltd, UK).

A JSM – 7401F field emission gun scanning electron microscope (FEG-SEM) machine (JEOL, Japan) was used to image the volar, dorsal and cross-sectional aspects of the samples, at $0^o$ and $30^o$ of tilt, at an EHT of 3kV and at a range of magnifications.

**2.6.2 Micro Computed Tomography**

Micro computed tomography (CT) scanning was chosen to assess tissue porosity. Unperforated and laser-perforated porous polymer samples were dried using a CPD and scanned using a micro CT scanner (Skyscanner 1172; Bruker, Belgium) at a resolution of 2µm, at a rotation step of $0.3^o$ and random movement setting of 20. Images were reconstructed using Skyscan NRecon reconstruction software (Bruker, Belgium) and processed using CTVox volume rendering software (Bruker, Belgium).

Quantitative data (e.g. open porosity), were calculated via CT-analyser software (Bruker, Belgium), over a designated region of interest selected at random.

**2.6.3 ImageJ Quantitative Analysis of Images**

Measurements of inter-perforation distance and perforation diameter were taken from FEG-SEM images of laser-perforated samples using ImageJ analysis software (National Institutes of Health, US) [22]. These were taken on days 0 and 15, over which period samples were incubated under PBS, changed 3 times weekly. For each perforation, 2 diameter measurements were taken in the horizontal (H) and vertical (V) planes. Interperforation distance was measured from one end of a perforation to the corresponding end of an adjacent perforation (n=17).

**2.7 Effect of Incubation and Time on Perforations**

Porous and non-porous laser and mechanically-treated samples were divided into 2 groups. One group was coated and imaged on day 0. The second group was stored under sterile phosphate-buffered saline (PBS, Sigma-Aldrich, US) and incubated for 15 days and imaged on day15. Perforation diameter was measured, at days 0 and 15, using FEG-SEM images of dorsal and volar aspects of laser perforations at both intensities. For each perforation, 2 diameter measurements were taken in the horizontal (H) and vertical (V) planes.

Figure 2 depicts the series of experiments undertaken.

**2.8 Cellular Studies**

**2.8.1 Cell Culture and Seeding**

All disposable materials used for cell culture were manufactured by Gibco™, ThermoFisher Scientific, UK unless otherwise stated.

Porcine epithelial cells (PEC) and P7072 porcine fibroblasts (PF) were obtained from a GMP-accredited lab (Laboratory of Cellular Therapeutics, Royal Free Hospital) and were isolated from piglet supraglottis. Murine fibroblasts (MF) from a 3T3 J2F cell line were cultured as a feeder layer for the PEC. All cells were cultured using standard cell culture techniques using a 10% solution of foetal bovine serum (v/v; FBS) in Dulbecco's modified Eagle's medium (DMEM).

Cells were cultured (Nunc™ Cell Culture Treated EasYFlasks™, Filter Cap; ThermoFisher Scientific, UK) at a seeding density of $1.0\times10^4 cm^{-2}$ and left to incubate over 24 hours to allow them to become adherent prior to medium change. The cells were then left to incubate with medium being changed approximately every 72 hours.

100µl of Mitomycin-C (1 mg/ml) was added to each flask to generate mitotically inactive feeder cells and after rinsing with PBS, ethylenediaminetetraacetic acid 0.02% solution (EDTA; 6ml; Sigma-Aldrich, US) was added and the cells incubated for 20 minutes The PEC were removed using TrypLE™ Select (1×; 10 ml; Gibco™, ThermoFisher Scientific, UK) and 20ml of media supplemented with Rho-associated coiled coil forming protein serine/threonine kinase (ROCK) inhibitor (0.1% v/v ROCK inhibitor in Ham's F12 Nutrient Mixture [23] [Gibco™, ThermoFisher Scientific, UK]) was then added.

After 1 week of culturing, TrypLE™ Select (1×; 10ml; Gibco™, ThermoFisher Scientific, UK) was added to digest the fibroblasts and PEC and the feeder cell layer removed. Supplemented DMEM was then added to inhibit TrypLE™ Select's action.

The cells were suspended in 40ml of Ham's F12 Nutrient Mixture [23] [Gibco™, ThermoFisher Scientific, UK]) and the cell densities of each mixture were established using a haemocytometer. Cells were cultured onto POSS-PCU scaffolds, previously sterilised by autoclaving, at a density of $3.31\times10^6$ cells/ml and $6.37\times10^6$ cells/ml for the PEC and PF respectively.

**2.8.2 Cell Proliferation and Viability**

The metabolism of cells seeded onto the surface of each scaffold was quantified via AlamarBlue® (ThermoFisher Scientific, UK) assay at selected time-points; day 1, 3 and 7 post-seeding, chosen to coincide with significant patterns in cell proliferation described in the literature [24].

15µl of AlamarBlue® was added to each sample-containing well of a 96-well culture plate to form a 10% AlamarBlue® and medium solution (v/v). The culture plate was incubated for 4 hours, after which the 150µl AlamarBlue® solution supernatant was aspirated and transferred to a fresh, tin-foil wrapped, 96-well culture plate. Fluorescence was measured using a Fluroskan Ascent FL (Thermo Labsystems, US) fluorescence microplate reader at 530nm excitation and 620nm emission wavelengths. Non-cell-seeded counterparts to each sample acted as controls.

**2.8.3 Histological Analysis**

Histology was used to assess cell migration into perforated POSS-PCU. Non-porous, porous, non-perforated and perforated scaffolds were transferred to a 96-well cell culture plate and cells cultured on the scaffolds for 13 days. The samples were then fixed overnight in 100% formaldehyde, for embedding, sectioning and staining.

They were then transferred to individual histocassettes (Sakura, US) and fixed in 10% neutral buffered formalin (NBF; 4% final formaldehyde) in closed pots for 24 hours at room temperature. The NBF was removed and replaced with PBS and the samples stored at 4$^{o}$C until ready for processing.

Processing to paraffin wax was conducted in an Excelsior AS automated tissue processor (Thermo Scientific, UK), using a standard over-night programme. The samples were dehydrated using 6 grades of ethanol and 4 grades of xylene, before being infused with paraffin wax (Sakura, US). They were then cut in half using a scalpel and each half embedded, in a cut surface down orientation, in individual paraffin blocks, using a Leica EG1140 H embedding station (Leica Biosystems, US). The first block of each half was then used to cut (without trimming) 2 × 4 ribbon sections using a Leica RM2135 microtome and Sakura blades. After using a heated water bath to elongate and non-coated glass slides, sections 1 – 3 and 4 – 7 were placed on two individual slides and stained using haematoxylin and eosin (H&E) using a Leica Autostainer XL, using a standard run protocol.

The stained slides were then scanned at ×40 magnification using a NanoZoomer NDP system (Hamamatsu, Japan), and displayed using NDP.view 2 software (Hamamatsu, Japan). They were also viewed under an inverted microscope (TMS-F, Nikon, Japan) at ×10 magnification and then imaged using Inifinty Analyze (Lumenara Corporation, Canada) software.

Figure 3 depicts the main stages involved in the cellular studies.

**2.9 Statistical Analysis**

Statistical analyses were performed via GraphPad Prism 7 software (GraphPad, US). A Mann-Whitney U test, Kruskal-Wallis test with Dunn's correction for multiple comparisons where relevant, or a two-way analysis of variance (ANOVA) with Sidak's multiple comparisons test where relevant, was used to analyse data for statistical significance. Statistical significance was considered as a p-value $<0.05$.

## 3. Results and Analysis

### 3.1 Characterisation of Porous POSS-PCU

#### 3.1.1 Surface Wettability

Porous scaffolds demonstrated an increase in contact angle which was however, statistically insignificant and which only changed minimally 6 months post-synthesis.

#### 3.1.2 Scanning Electron Microscopy

SEM was used to image the volar, dorsal and cross-sectional surfaces of the unperforated scaffolds (Figure 2). These included non-porous, porous and porous, 6 months post-synthesis, samples.

An impermeable 'skin' was present on the dorsal and volar surfaces of the scaffolds (Figures 2A and 2C) with an inner substructure consisting of a network of interconnected pores in cross-section (Figure 2B). Whilst the dorsal surface was smooth (Figure 2A), the volar surface had a 'cobblestone' appearance (Figure 2C). The non-porous sample had no holes whereas the porous bore a number of sporadic, irregularly shaped holes that varied in size. The holes found on the volar surface had the appearance of a 'burst bubble,' whilst those on the dorsal edge were crater-like and did not appear to provide access to the porous substructure. No morphological differences were noted between porous scaffolds synthesised 6 months apart.

### 3.2 Altering POSS-PCU Surface Topography

Figure 3 demonstrates the changes in POSS-PCU surface topography as a result of the mechanical and laser techniques. These are discussed in greater detail below.

#### 3.2.1 Field Emission Scanning Electron Microscopy

Images were taken of the volar, dorsal and cross-sectional surfaces of the polymer scaffolds which had undergone the laser and mechanical techniques (Figure 4). The morphology of these scaffolds correlated well with that of the non-perforated samples imaged previously (Figure 2).

Perforations were not visible on any of the scaffold surfaces which underwent the mechanical method (Figures and C). Crushing of the substructure did not appear to have taken place, even at the higher force (Figure 4B). At higher magnification, modification of the surface topography was visible, becoming more textured and effectively increasing surface area (Figure 4C).

Both porous and non-porous scaffolds which had undergone the laser technique exhibited ovoid-shaped perforations which had penetrated through the entire thickness of the polymer (Figure 4D). In terms of organisation, the laser-cut holes were arranged in an orderly fashion (Figure 4F) and mean inter-perforation spacing was approximately 1.4mm. The diameter of the laser-cut holes, on the other hand, was variable, with holes appearing wider on the surface and narrowing as they tapered down into the polymer (Figures 4F and 4D). The exit-hole at the base had an everted edge (Figure 4E).

#### 3.2.2 Micro Computed Tomography

Micro computed tomography (μCT) images were taken of the porous, unperforated and laser perforated scaffolds were taken (Figure 5). All images in this section are represented by a colour bar, with a scale from white (65535 - low density) to black (0 - high density). Figure 5A highlights the impermeable 'skin' on the dorsal and volar aspects of the unperforated POSS-PCU scaffolds. This denser material appears dark red/black.

μCT images of the scaffolds which underwent the laser technique showed surface perforations at regularly spaced intervals. Figures 5B and 5C exhibit 2 laser perforations made at intensity 6. These show the inner walls of the perforations and how they allow access to the interconnected porous substructure of the scaffold. The perforations appear to have an everted edge on the dorsal surface (Figure 5D) of the polymer.

Figure 5B shows that even at the higher intensity setting (6), the laser did not cauterise and seal off the inner walls of the perforations.

### 3.2.3 Micro Computed Tomography Data

Micro CT was also used to generate quantitative data, comparing the porosity of the unperforated and perforated, porous scaffolds (Table 3). As expected, the porous, laser-perforated scaffolds, exhibited values of total porosity and open porosity which were greater than those of the unperforated, porous sample. Porous POSS-PCU perforated at intensity 3 achieved a higher total porosity in comparison to that perforated at intensity 6. However, it also demonstrated a higher closed porosity value. This shows that whilst the scaffolds, which were laser perforated at intensity 3, had a higher total porosity, these pores were not as well connected as those of the scaffolds perforated at intensity 6, giving rise to a higher number of closed pores. Our porosity data also highlighted that closed porosity only forms a relatively low percentage of total porosity.

## 3.3 Cellular Compatibility

### 3.3.1 Cell Proliferation

Figure 6 illustrates the metabolic activity patterns produced following cell-seeding of non-porous, porous, unperforated and laser perforated scaffolds.

Unperforated scaffolds demonstrated an immediate and overall decline in metabolic activity, for both porous and non-porous samples, showing that the unperforated scaffolds are incompatible with cell viability. The laser perforated, non-porous samples also resulted in an overall decrease in cell metabolic activity, particularly between days 3 and 7. In contrast, perforated, porous POSS-PCU scaffolds demonstrated an increase in metabolic activity between days 3 and 7 which was more pronounced for those perforated at laser intensity 6.

### 3.3.2 Histology

Haematoxylin and Eosin (H&E) staining of sections taken from cell-seeded scaffolds confirmed the presence of cells in and around the scaffolds (Figure 7). Cells were seen to be adherent to the scaffold surface. Figures 7A and 7B show cells and debris within large depressions in the scaffold surface, representing cells located inside laser perforations. Furthermore, cells were seen within large pores, located within the scaffold's substructure, indicative of cellular migration into the scaffold (Figure 7C).

Images of sections with no surface perforations showed the presence of cells adjacent to the scaffold but not within it. Figure 7D shows that when scaffolds with no obvious perforations were seeded with cells, no cells were seen to have entered into the scaffold's porous substructure.

## 3.4 Young's Modulus of POSS-PCU

Figure 8 demonstrates Young's Modulus of non-porous, porous, unperforated and perforated POSS-PCU scaffolds. The non-porous polymer showed the lowest stress and the highest strain at break and the lowest Young's Modulus. The incorporation of porogen to form the porous scaffolds also increased the Young's Modulus of the material. However, comparing porous scaffolds synthesised 6 months apart demonstrated a reduction in Young's Modulus with time.

Surface modification by the laser and mechanical techniques further increased Young's Modulus. By day 15, all laser-perforated samples showed a reduction in Young's Modulus. This reduction was noticeably greater for the porous samples. The scaffolds which underwent mechanical modification at a force of 2.6N also showed a reduction in Young's Modulus by day 15, whereas those modified at a force of 5.2N demonstrated an increase.

## 3.5 Narrowing of Perforations with Time and Incubation

FEG-SEM at higher magnification (Figure 9) was used to obtain more detailed images of the laser perforated, porous scaffolds at both intensities. Perforations were noted to be ovoid in form but irregularly shaped.

Figure 9D shows changes in perforation diameter, taken from samples on days 0 and 15, to investigate changes in morphology caused by the polymer's stress relaxation behaviour which causes the diameter of the perforations to decrease over time. The

results demonstrate a reduction in mean diameter (339.8µm ± 14.5 to 301.6µm ± 14.0) over a 15 day period. The morphology of the perforations changed from ovoid to more circular in shape during the relaxation.

**4. Discussion**

The development of scaffolds with material characteristics that support very different internal and external environments and biological demands, such as epithelialisation, would represent a step-change in our ability to reconstruct hollow organs, such as larynx and oesophagus. The implantation of such scaffolds may attain an increased success rate by ensuring little or no difference between the Young's Modulus of the scaffold and that of the native tissue, adequate cellular adhesion, angiogenesis and tissue integration into the porous scaffold [25]. Whilst one of the major aims of POSS-PCU scaffolds in tissue engineering of hollow viscera is that of maintaining structural support [9] and barrier function [26], another is to promote tissue and vascular regeneration [17, 18]. Optimising the material's internal and surface porosity can encourage this process, thus aiding cell migration into the scaffold substructure to improve clinical delivery. Here we describe the introduction of surface pores to coagulated POSS-PCU scaffolds and the effect of this modification on the polymer's properties.

Prior to perforating POSS-PCU's surface, we confirmed that the addition of porogen to produce the porous polymer did not significantly affect its surface wetness, which implies that it did not alter surface chemistry. Using SEM, we demonstrated that porous-POSS-PCU has improved internal porosity, an important characteristic as successful *in vivo* cell and tissue growth, upon transplantation, are reliant on this [27]. Our SEM images also showed that although the porous scaffolds possess open surface pores, these are small and sporadic. Such pores are therefore unlikely to substantially increase the ability of cells to migrate into the scaffold since large cells, such as fibroblasts (50-100 µm), are unable to pass through a smaller gap [28]. Previous studies indicate that pores of 40µm – 600µm offer optimal conditions for capillary angiogenesis into scaffolds [29]. Altering POSS-PCU surface topography to increase the number and size of pores is therefore desirable.

Using the laser technique we succeeded in creating surface pores on POSS-PCU whilst simultaneously increasing its internal porosity using porogen. We confirmed that laser-cutting succeeded in creating pores without cauterising the surface of the inner walls and which penetrated through the entire thickness (approximately 300µm) of the scaffold. This provided a conduit, connecting the polymer surface to the porous substructure. Additionally, micro CT scans confirmed that the pores, now open to the external environment, did indeed connect freely with the internal, porous substructure of the scaffold. Porosity is known to be critical to successful scaffold application and functionality [17].

Whilst the lower-intensity laser technique demonstrated the highest total porosity (96.4%), POSS-PCU scaffolds perforated at the higher intensity still achieved a near-optimal total porosity of 89.5%, necessary for cell-seeding and ingrowth [30]. However, porosity is not the only consideration when addressing scaffold design. Cellular migration, circulation of extracellular nutrients and cell signals are all augmented by pore interconnectivity [31]. Notably, we showed that the laser-perforated, porous POSS-PCU network displayed excellent interconnectivity with the percentage of closed porosity representing only a minimal fraction of the overall porosity. Furthermore, we demonstrated that POSS-PCU perforated at the higher intensity had a lower number of closed pores, whilst that perforated at the lower intensity had the highest degree of closed porosity. Therefore, despite not achieving higher total porosity, the higher laser intensity could produce the more desirable scaffold design. Although high porosity facilitates biofactor release and enhances nutrient exchange [17], it often comes at the expense of the structural stability of the polymer [13]. This is a major challenge in tissue engineering of hollow organs as they must possess the mechanical strength and rigidity to withstand intraoperative handling and *in vivo* loading [30] and to prevent collapse [32]. An optimal laser intensity would therefore be one which achieves a near-ideal porosity, with a high level of connectivity but with minimal compromise of the scaffold's structural integrity. Our work opened up interesting avenues for further research using different laser intensities, aiming for an ideal balance between these factors. It would also be useful to investigate which would be the more ideal mean pore size to achieve. Whilst pores which are too small restrict cell migration, pores which are unnecessarily large decrease the scaffold's surface area thereby limiting cell adhesion [33].

As cell numbers affect cell confluency which in turn influences the cell differentiation process [34], we used cell proliferation studies to obtain preliminary data appraising whether perforating POSS-PCU's impermeable surface would improve cell migration into the scaffold's substructure, reflected by an increase in cell numbers and metabolic activity [35]. Our data showed a marked contrast between the metabolic activity patterns exhibited by perforated and unperforated POSS-PCU scaffolds. The latter showed a steady decrease in metabolic activity, suggesting a reduction in total cell numbers or in their metabolic rates, for instance due to quiescence. This supports the premise that the unperforated polymer surface is not optimal for cell viability due to a reduced capacity for cells to enter the scaffold. Notably, unperforated scaffolds, whether porous or non-porous, gave similar results reinforcing that it is the lack of access to the porous substructure which is the limiting factor for cellular proliferation and possible epithelisation. Additionally, metabolic activity for perforated but non-porous scaffolds fell to levels below those achieved by their porous counterparts, highlighting that internal porosity is also critical for cell viability.

The laser perforated, porous scaffolds demonstrated patterns of metabolic activity against time which are generally compatible with those reported in literature [24, 34]. Divieto and Sassi [24] used highly porous Biocoral® scaffolds with well-connected pores, presenting no obstacle to cell migration. We used similarly-sized scaffolds and densities of $3.63\times10^5$ cells/scaffold. From Divieto and Sassi's study, it appears that cells seeded at low densities grow consistently, whilst those seeded at densities higher than $1.0\times10^3$ cells/scaffold (as in this study) fluctuate over time. A large number of cells are able to fill pore spaces rapidly but then decrease proliferation rate due to cell-contact inhibition. This 'lag phase' is then followed by an increase in metabolic activity as cells fill a new pore and proliferate [24]. Our results reflected this pattern. We therefore inferred that laser-perforated, porous POSS-PCU was able to support viable cell growth in contrast with unperforated controls, although further investigations, such as cell proliferation and differentiation studies, would be required to confirm this.

An interesting facet of this study was to compare the effects of the two intensities of laser used. The porous scaffolds perforated at the higher laser intensity demonstrated a steeper increase in metabolic activity compared to the lower intensity. This indicates a faster rate of proliferation, correlating with the increased interconnectivity achieved at the higher intensity discussed earlier. This reinforced our premise that a more ideal scaffold is produced by the higher laser intensity.

Perforated POSS-PCU histology showed cells adherent to the scaffold surface, illustrating that cells seeded onto the scaffold were able to attach to its surface and remain viable, rather than undergo anoikis. Importantly, our results also showed cells aggregated within perforations and infiltrated into the polymer. These findings show that cells aggregate in large perforations and demonstrate that perforating POSS-PCU's surface facilitated cellular infiltration into the scaffold. In contrast, the absence of perforations was accompanied by an absence of cells within the scaffold. This emphasises that perforating POSS-PCU's surface encourages cell migration, instigating increased tissue ingrowth *in vivo*, crucial for angiogenesis and interlocking of the scaffold with the native tissue[17]. Further work on epithelialisation would be necessary as prompt re-epithelialisation is an important factor for optimal wound healing [36], which in turn reduces the incidence of infection [37]. Moreover, epithelial tissue forms the inner lining of hollow organs such as the larynx, where it is important for effective barrier functionality and for maintaining homeostasis [38, 39]. It is known that, at present, untreated, synthetic scaffolds are not well suited to support epithelisation [40].

Cell adhesion is an essential preliminary step to subsequent proliferation [41] and an ideal scaffold should therefore promote a high level of cell attachment besides optimal scaffold infiltration. The inverse relationship between pore size for cell migration, and surface area available for cell attachment, is well-documented [42, 43]. Whilst the mechanical method did not appear to have perforated POSS-PCU's surface, it did alter its topography, effectively increasing its surface area. An interesting, synergistic way forward may be combining both laser and mechanical methods to maximise their potential. In this way, the mechanical technique may increase surface area to redress that lost by laser perforation. The mechanical method did not result in crushing of the porous substructure calling for further investigation at higher forces.

Synthetic polymers have the advantage of possessing reproducible and precise mechanical and physical properties [44]. These include tensile strength and elastic modulus, both important scaffold characteristics for intraoperative handling and cellular differentiation [45]. POSS-PCU has been found to be superior to other synthetic materials in terms of its mechanical properties and elastic modulus [41]. It also has the potential to be modified to produce an elastic modulus more closely simulating that of native tissue [25]. The larynx presents a challenge in TE since it possesses different components with different mechanical properties. Our data showed that the addition of porogen raises Young's Modulus (Non-Porous, Unperforated = 1.20 and Porous, Unperforated = 1.77) and this is further elevated by laser perforation (Porous, Laser-Perforated, Intensity 6 = 1.86; Porous, Laser-Perforated, Intensity 3 = 2.38) to more closely resemble that of human cadaveric cricoid cartilage (2±0.9), established by Baiguera et al. [46].

Importantly, we showed that this increase in Young's Modulus reverses with time, decreasing substantially over a 15 day period. We also demonstrated that when POSS-PCU scaffolds were incubated at 37ºC (simulating *in vivo* conditions) average pore diameter contracted by just over 11% over a 15 day period, correlating with the diminishing Young's Modulus observed over time. The perforation morphology also changed from ovoid to a more circular appearance. These findings may be explained by a relaxation of the polymer caused by incubation conditions or by the polymer's innate elastic properties. The result is narrowing of the perforations with time. A diminishing surface pore size could have a detrimental effect on cell infiltration into the scaffold since small pores restrict cell migration leading to the development of cell aggregates. These form a cellular skin around the scaffold surface effectively limiting the diffusion of nutrients and waste material, producing necrotic areas within the scaffold [28, 33]. The changes observed in Young's Modulus and perforation diameter are critical as they affect the scaffolds physical properties. A native tissue-scaffold mismatch in mechanical properties has been proposed in the literature as a negative prognostic factor for scaffold integration [47]. It may also further contribute to the formation of granulation tissue at the anastomotic site [48]. This raises important questions regarding how time and the conditions to which POSS-PCU is subjected,

affect its properties. An important goal of TE is ‘off-the-shelf’ availability, which is a major advantage of synthetic scaffolds. It is therefore important to consider how our findings relate to POSS-PCU scaffold ‘shelf-life,’ and to the conditions under which it should be stored, as well as potential post-implantation issues, all of which are of paramount importance to the translatability and clinical application of POSS-PCU.

**Conclusion**

Our findings demonstrate that besides internal porosity and interconnectivity, surface perforations are critical in influencing cell behaviour in POSS-PCU scaffolds. Initial cell seeding density also affects cell proliferation patterns. Future research should address the possibility of correlating these parameters with resultant cell numbers. In addition to using porogen, perforating the POSS-PCU surface can be utilised to encourage migration and proliferation under controlled conditions. Furthermore, the properties perforations lend to the scaffold could lead to improved anchorage to the native tissue which, by decreasing the possibility of implant dislodgement, may increase the likelihood of successful and complication-free post-operative outcomes for future patients receiving hollow organ implants.

**Acknowledgements**

The authors would like to thank Dr Angela Tait, Dr Toby Proctor and the staff at the Royal Free Hospital Laboratory of Cellular Therapeutics, for providing some of the laboratory resources and facilities for this study; Mr Mark Hopkinson at the Royal Veterinary College for his assistance with micro CT imaging and data analysis; the staff at the Pathology Core Facility Service, UCL for assistance with histology; Mr Mark Turmaine for assistance with scanning electron microscopy; and Dr Hazel Welch and the staff at the Division of Surgery for helpful discussion and guidance.
Funding Sources

This work was supported by the Medical Research Council (MR/K026453/1, MAB and NM); Division of Surgery and Interventional Science, University College London (MLMSC, KW).

**Ethical Standards**

The authors state that this research did not involve any human or animal experimentation.

**Tables and Figures**

| Material | Perforation Method | Intensity/Force | Code |
|---|---|---|---|
| Non-Porous | Unperforated | N/A | C |
| Non-Porous | Mechanical | 2.6 N | CF3 |
| Non-Porous | Mechanical | 5.2 N | CF6 |
| Non-Porous | Laser | 3 | CP3 |
| Non-Porous | Laser | 6 | CP6 |
| Porous | Unperforated | N/A | T |
| Porous | Mechanical | 2.6 N | TF3 |
| Porous | Mechanical | 5.2 N | TF6 |
| Porous | Laser | 3 | TP3 |
| Porous | Laser | 6 | TP6 |

**Table 1. Description of POSS-PCU samples** used in the various experiments.

| Sample | Contact Angle - θ (°) |
|---|---|
| Non-Porous | 80.0 ± 1.23 |
| Porous (Sample 2) | 91.4 ± 3.80 |
| Porous (Sample 1: 6 months post-synthesis) | 91.8 ± 2.23 |

**Table 2. Contact angle testing** on non-porous and porous unperforated scaffolds.

| Indices | Unperforated | Laser Perforated - 3 | Laser Perforated - 6 |
|---|---|---|---|
| Number of closed pores | 147 | 582 | 206 |
| Volume of closed pores ($mm^3$) | 0.00008 | 0.0004 | 0.00013 |
| Surface of closed pores ($mm^2$) | 0.0565 | 0.274 | 0.0946 |
| Closed porosity (%) | 0.0202 | 0.103 | 0.028 |
| Volume of open pore space ($mm^3$) | 2.91 | 10.5 | 4.1 |
| Open porosity (%) | 87.9 | 96.4 | 89.5 |
| Total volume of pore space ($mm^3$) | 2.91 | 10.5 | 4.1 |
| Total porosity (%) | 87.9 | 96.4 | 89.5 |

**Table 3. Pore analysis data** obtained through Micro CT comparing unperforated, porous POSS-PCU, with porous POSS-PCU perforated at laser intensities 3 and 6.

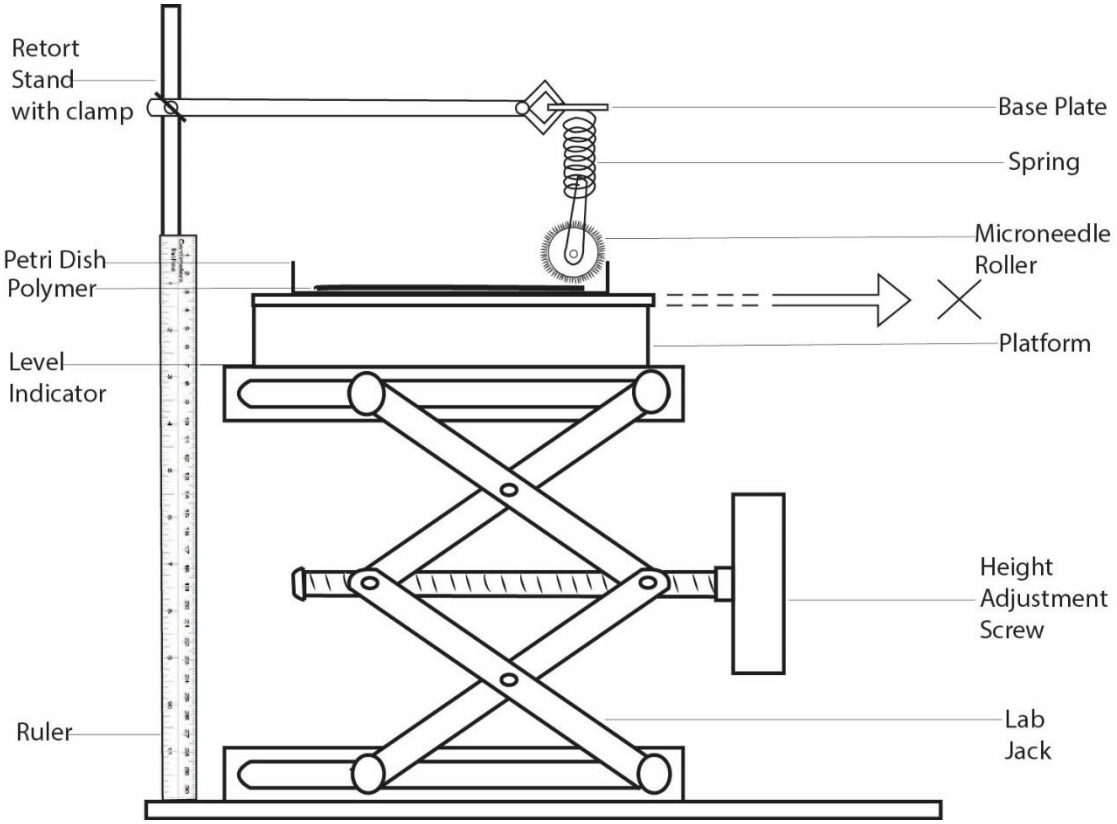


**Figure 1. Mechanical Perforator Apparatus Set-up.** The platform is equipped with a retractable drawer mechanism, on which the petri dish is mounted. X indicates the direction in which the retractable drawer is pulled.

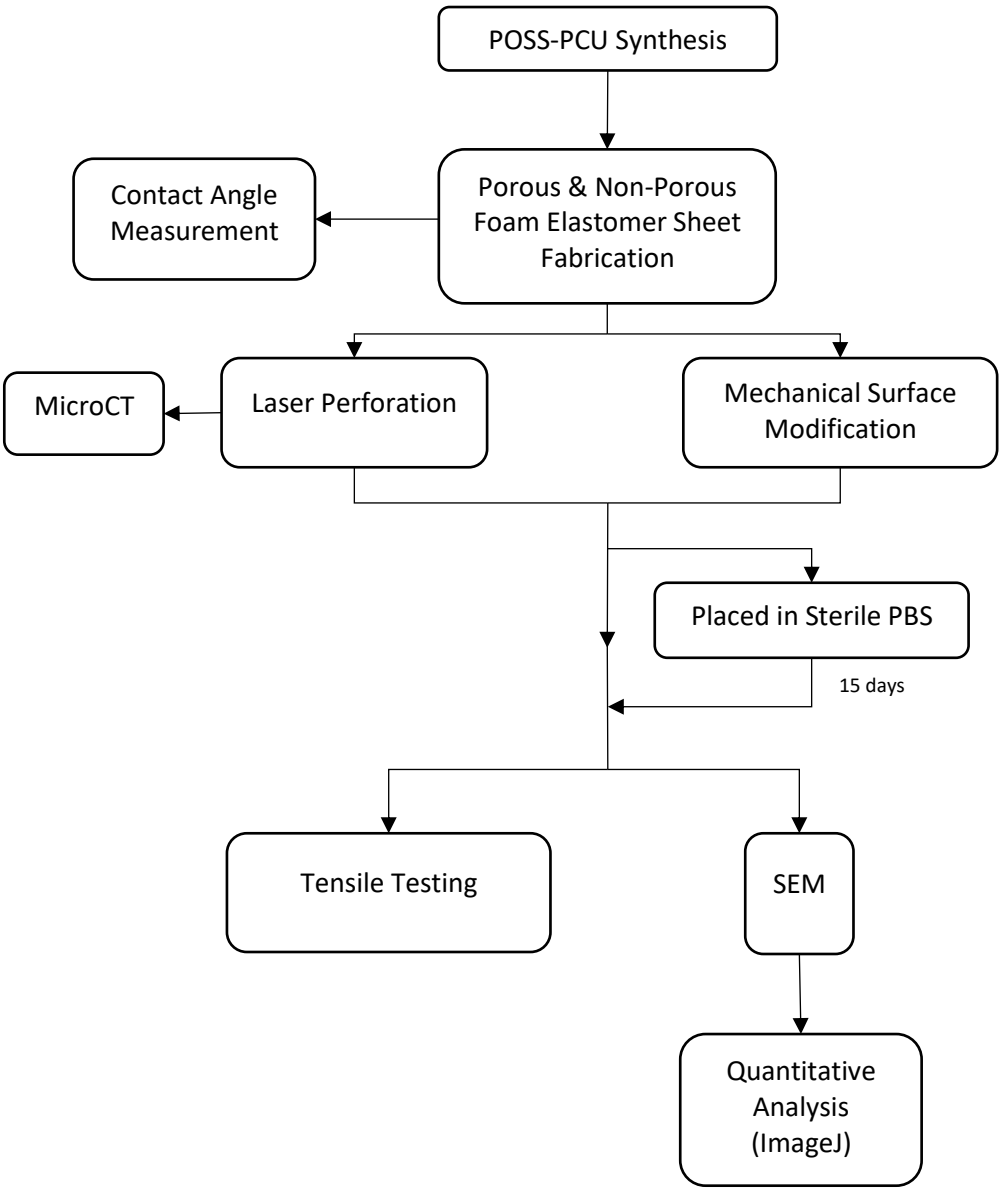


**Figure 2. Flowchart** summarising key steps and timelines of the characterisation experiments. Statistical analysis was also carried out.

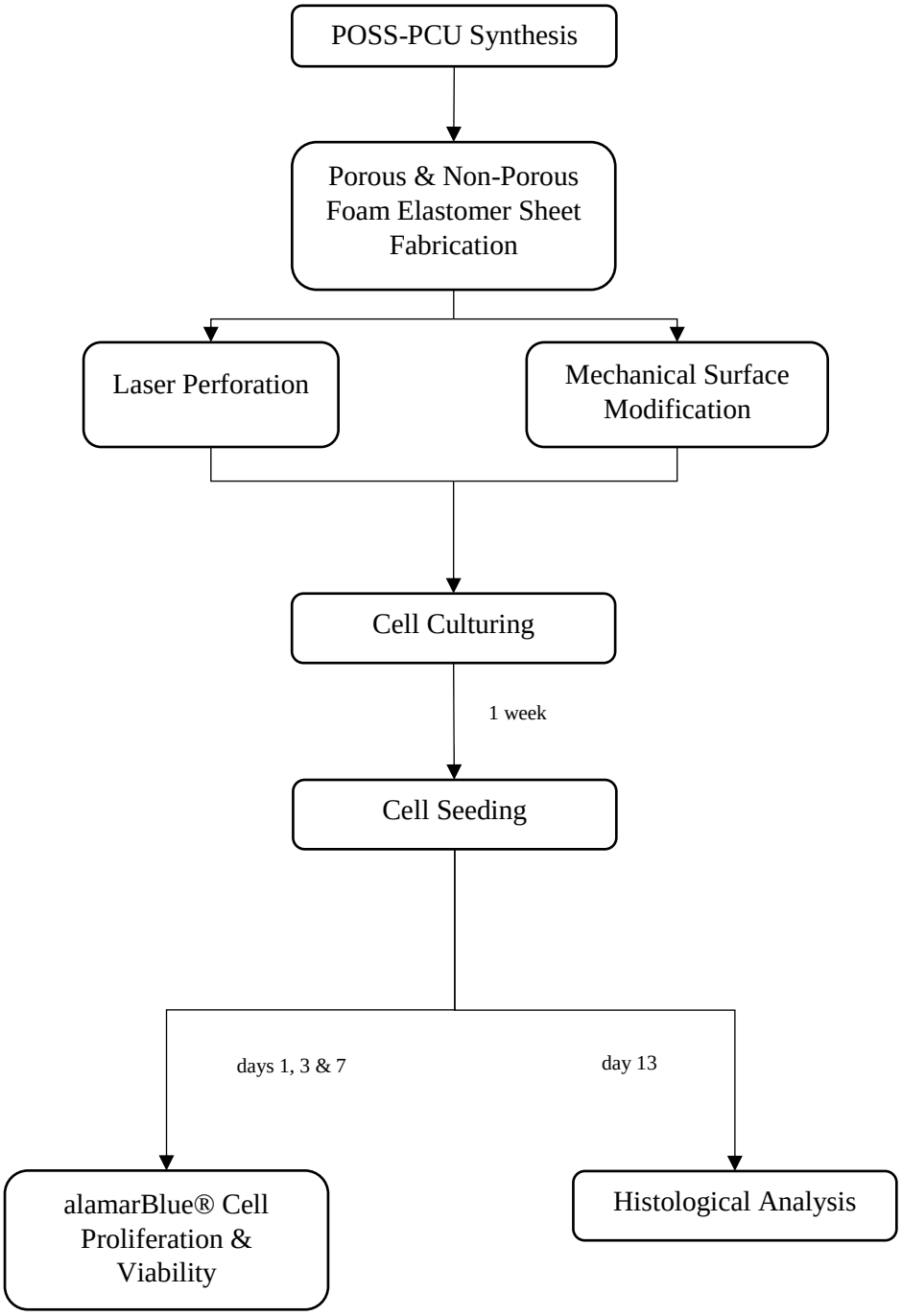


**Figure 3. Flowchart** summarising key steps and timelines of the experiments involving cellular studies. Statistical analysis was also carried out.

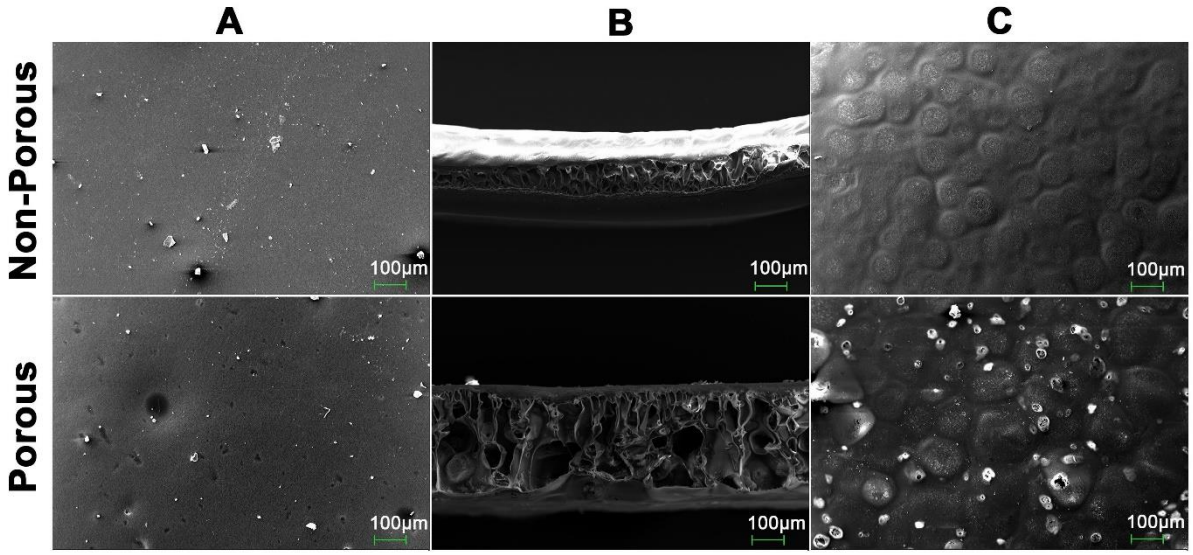


**Figure 4. SEM micrographs** of the dorsal (A), cross-sectional (B) and volar (C) surfaces of unperforated samples derived from non-porous and porous samples. Magnification x250 in all cases.

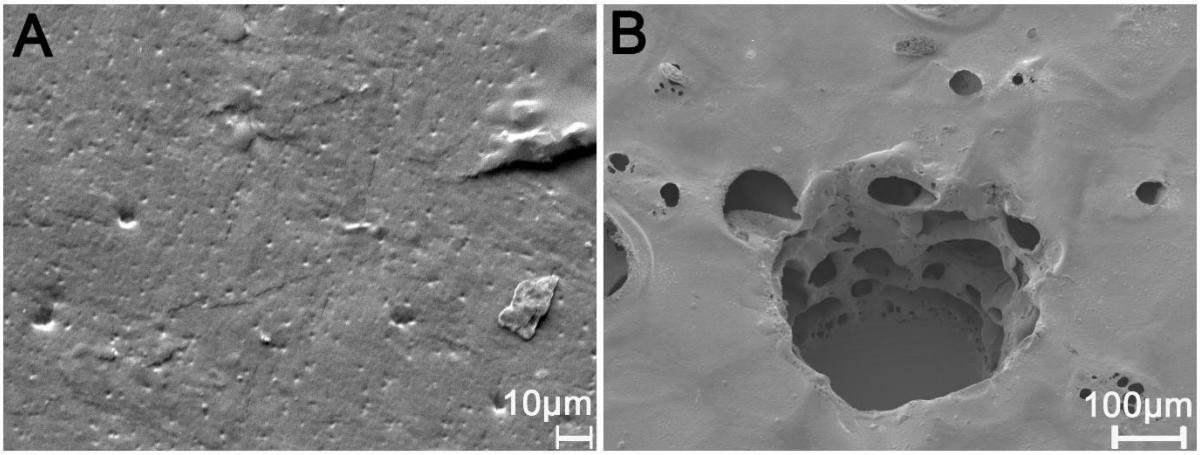


**Figure 5. FEG-SEM micrographs** depicting surface topography changes induced by the mechanical method (A) – Mag. X700 and the laser technique (B) – Mag. X150.

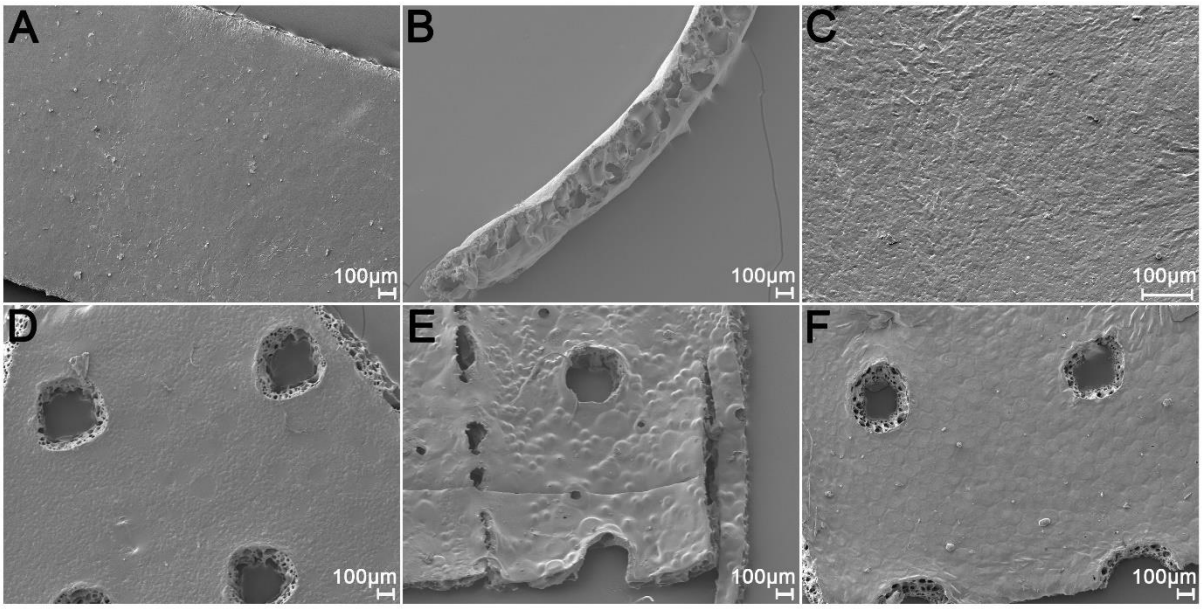

**Figure 6**. **FEG-SEM micrographs** taken on the day of perforation (day 0). These compare scaffolds which underwent the mechanical (A-C) and laser (D-F) techniques. Mag. X50.

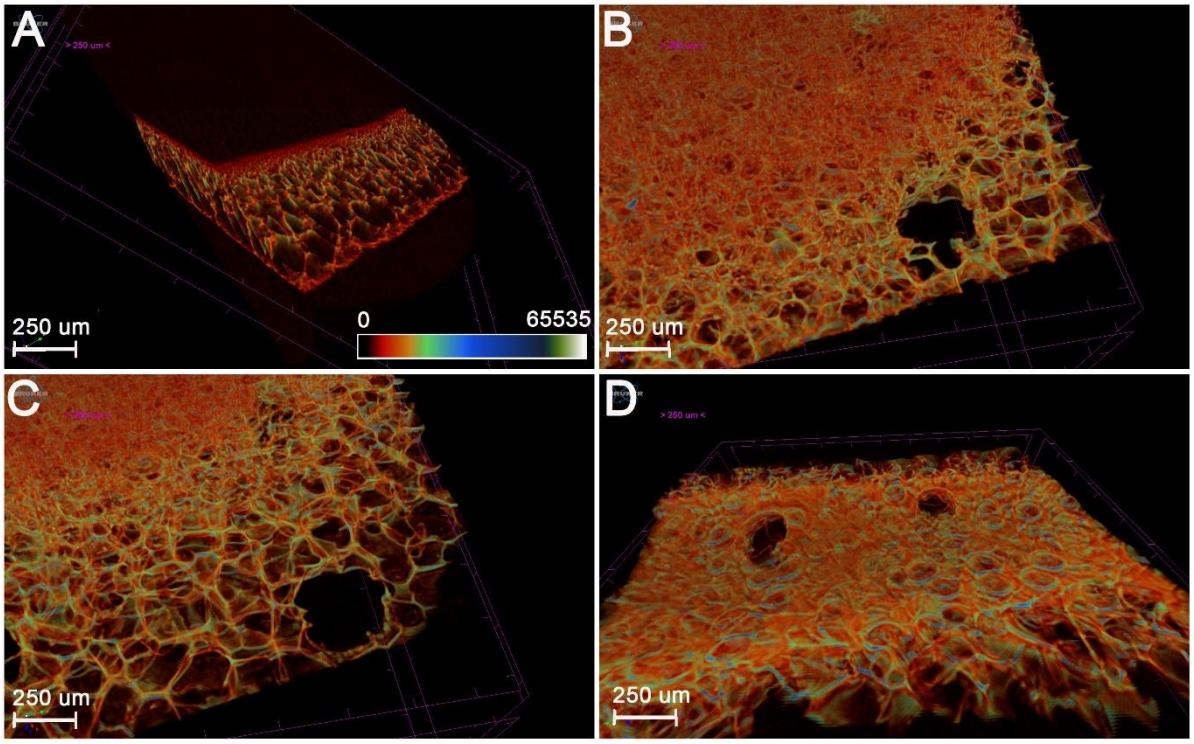


**Figure 7. Micro CT image** showing: an oblique cross-section through an unperforated, porous POSS-PCU scaffold (A), progressive longitudinal sections through a porous scaffold, laser perforated at intensity 6 (B and C) and 3 (D). Sections are taken from the volar (left) to dorsal (right) aspects.

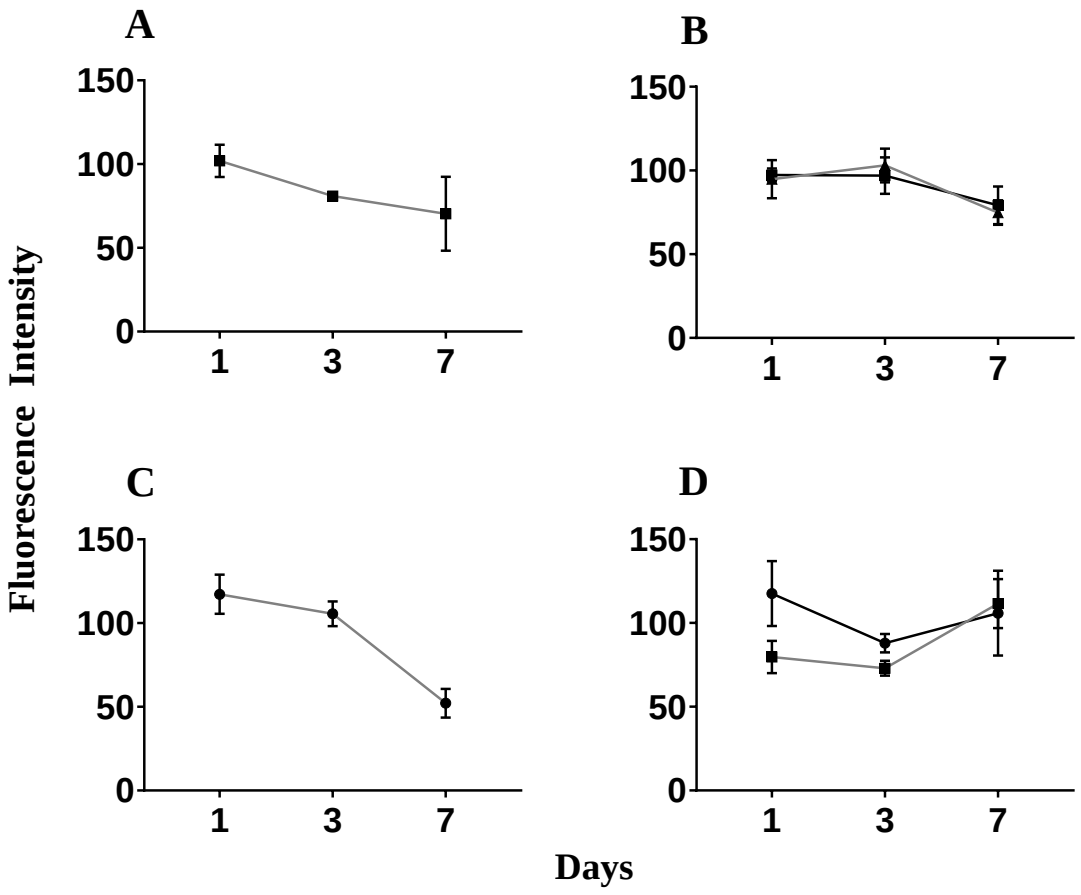

**Figure 8. Trends in metabolic activity** of porcine epithelial cells and fibroblasts seeded onto POSS-PCU scaffolds over days 1, 3 and 7. The graphs compare A – unperforated, non-porous; B – laser-perforated (intensities ■ 3 and ▲ 6), non-porous; C – unperforated, porous; D – laser-perforated (intensities ● 3 and ■ 6), porous. In all cases error bars represent standard error of mean and n=3.

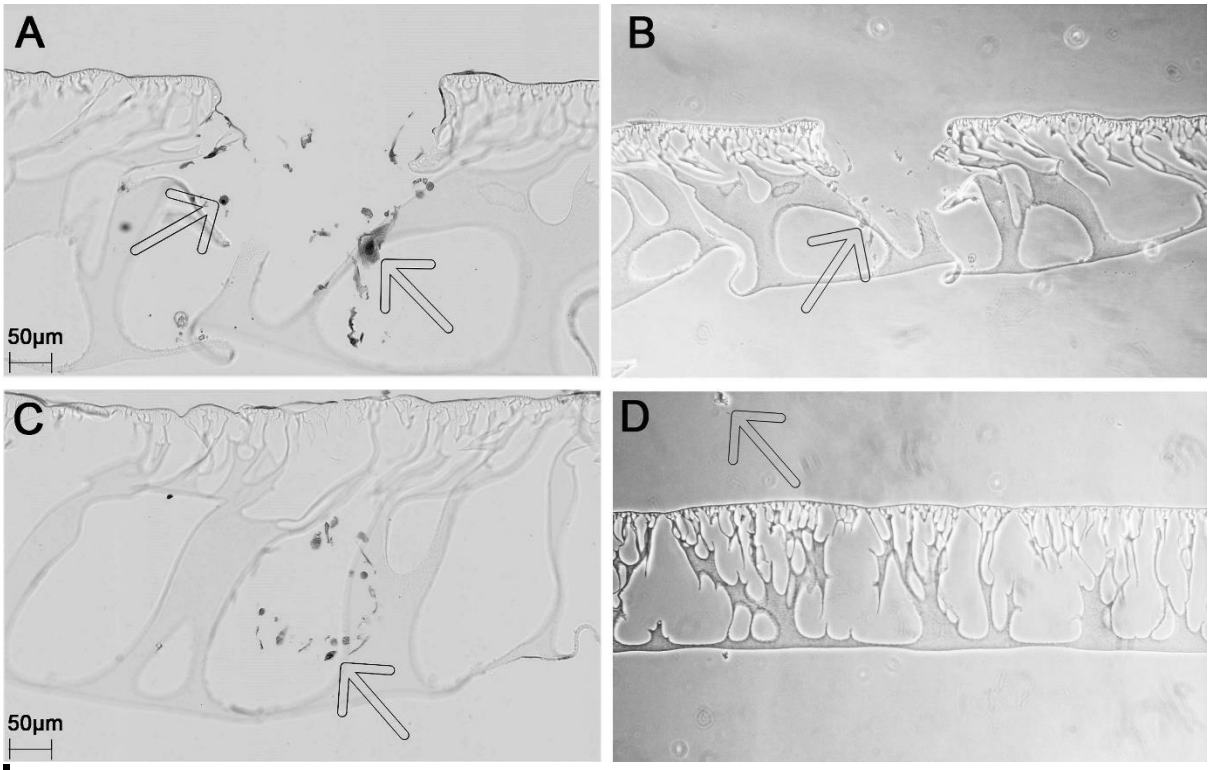


**Figure 9. Images taken from H&E-stained sections of POSS-PCU scaffolds seeded with cells.** Cells, indicated by arrows, and debris present within depressions in the scaffold's surface (A and B). Cells located within the scaffold's porous substructure with no obvious mode of entry, indicating migration into scaffold (C). Cells visible adjacent to the scaffold (arrow) but not within porous substructure indicate unperforated scaffolds are not conducive to intra-scaffold cell migration (D). Images A and C taken using a NanoZoomer NDP system and displayed using NDP.view 2 software, B and D taken using a TMS-F microscope and imaged using Infinity Analyze software. Magnification ×10.

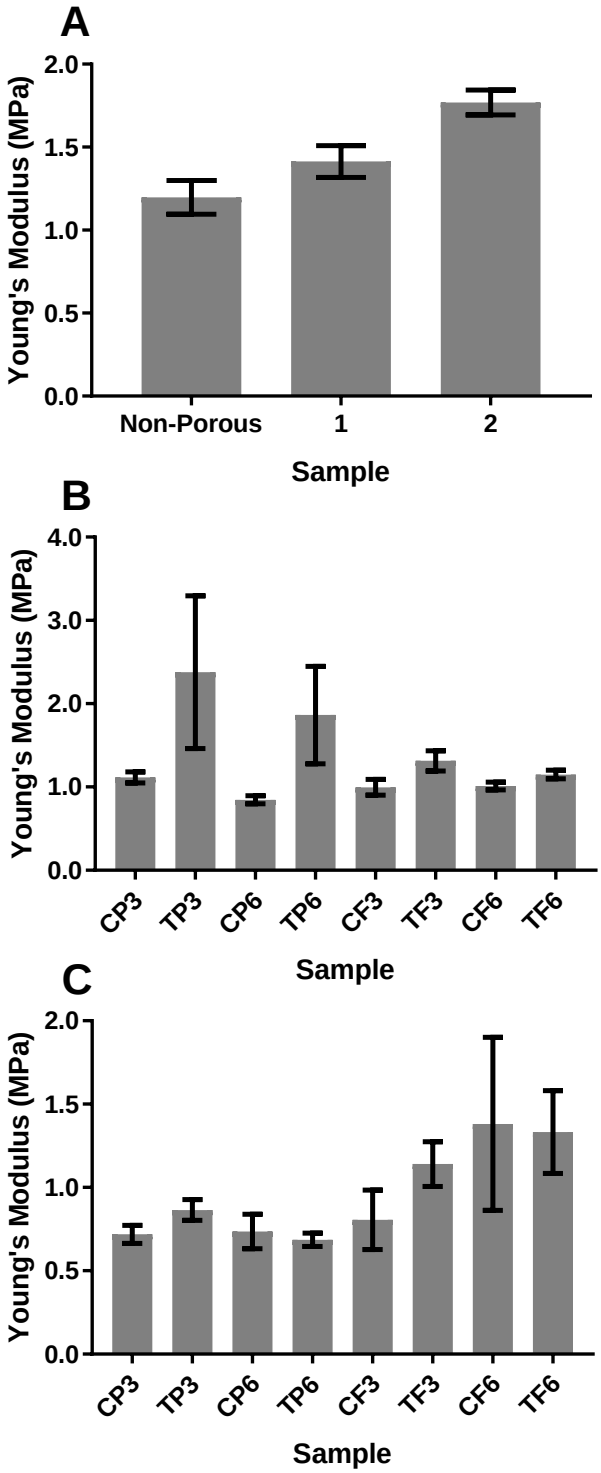


**Figure 10.** Young's moduli of A – unperforated: non-porous, porous (1) and porous 6 months post-synthesis (2) specimens; B – porous and non-porous samples which underwent the mechanical technique at 2 forces (2.6 N and 5.2 N) and laser-perforation at 2 intensities (3 and 6) on day 0; C – porous and non-porous samples which underwent the mechanical technique at 2 forces (2.6 N and 5.2 N) and laser-perforation at 2 intensities (3 and 6) on day 15. N=5 and error bars represent standard error of mean (SEM) for all samples.

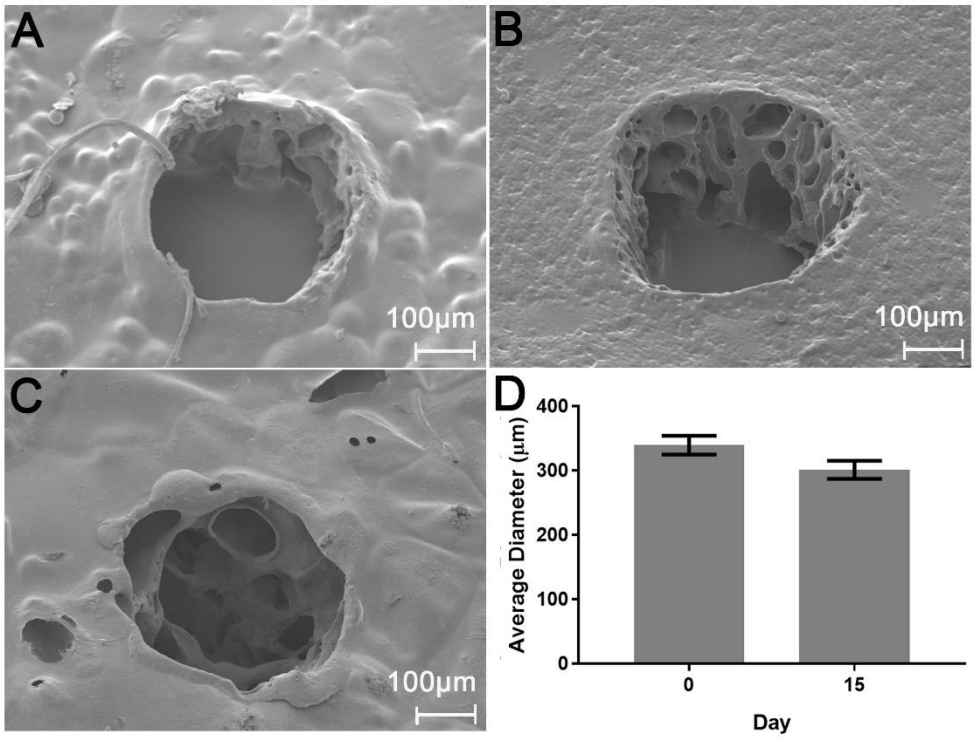


**Figure 11. FEG-SEM micrographs** of laser-cut perforations and measurement of their diameter at 2 time-points. A - day 0, intensity 3; B - day 0, intensity 6; C - day 15, intensity 3. Magnification x150. D - Comparison of means of perforation diameter of laser-cut holes at day 0 and day 15. Mean diameter at day 15 (301.6µm ± 14.0) is less than that at day 0 (339.8µm ± 14.5). Error bars represent standard error of mean.

**References**


1 Ansari T, Lange P, Southgate A, Greco K, Carvalho C, Partington L, et al. Stem Cell-Based Tissue-Engineered Laryngeal Replacement. *Stem Cells Translational Medicine* 2017;**6:**677-87

2 Ganly I, Patel S, Matsuo J, Singh B, Kraus D, Boyle J, et al. Postoperative complications of salvage total laryngectomy. *Cancer* 2005;**103:**2073-81

3 Ganly I, Patel SG, Matsuo J, Singh B, Kraus DH, Boyle J, et al. Analysis of postoperative complications of open partial laryngectomy. *Head Neck* 2009;**31:**338-45

4 Pereira da Silva A, Feliciano T, Vaz Freitas S, Esteves S, Almeida e Sousa C. Quality of Life in Patients Submitted to Total Laryngectomy. *J Voice* 2015;**29:**382-8

5 Agarwal SK, Gogia S, Agarwal A, Agarwal R, Mathur AS. Assessment of voice related quality of life and its correlation with socioeconomic status after total laryngectomy. *Annals of Palliative Medicine* 2015;**4:**169-75

6 Omori K, Nakamura TF-K, Shinichi, Kanemaru SF-A, Ryo, Asato RF-Y, Masaru, Yamashita MF-T, Shinzo, Tanaka SF-M, Akhmar, et al. Regenerative medicine of the trachea: the first human case. *The Annals of Otology, Rhinology & Laryngology* 2005;**114:**429-33

7 Laurance J. British boy receives trachea transplant built with his own stem cells. *Br Med J* 2010;**340:**c1633

8 Hamilton NJ, Kanani M, Roebuck DJ, Hewitt RJ, Cetto R, Culme-Seymour EJ, et al. Tissue-Engineered Tracheal Replacement in a Child: A 4-Year Follow-Up Study. *Am J Transplant* 2015;**15:**2750-7

9 Hamilton NJI, Birchall MA. Tissue-Engineered Larynx: Future Applications in Laryngeal Cancer. *Current Otorhinolaryngology Reports* 2017;**5:**42-8

10 Mehrban N, Zhu B, Tamagnini F, Young FI, Wasmuth A, Hudson KL, et al. Functionalized alpha-Helical Peptide Hydrogels for Neural Tissue Engineering. *ACS Biomater Sci Eng* 2015;**1:**431-9

11 Atala A, Kasper FK, Mikos AG. Engineering Complex Tissues. *Sci Transl Med* 2012;**4:**160rv12-rv12

12 Cunha C, Panseri S, Antonini S. Emerging nanotechnology approaches in tissue engineering for peripheral nerve regeneration. *Nanomedicine: Nanotechnology, Biology and Medicine* 2011;**7:**50-9

13 Hollister SJ. Porous scaffold design for tissue engineering. *Nature Materials* 2005;**4:**518-24

14 Knight PT, Lee KM, Chung T, Mather PT. PLGA–POSS End-Linked Networks with Tailored Degradation and Shape Memory Behavior. *Macromolecules* 2009;**42:**6596-605

15 Gupta A, Vara DS, Punshon G, Sales KM, Winslet MC, Seifalian AM. In vitro small intestinal epithelial cell growth on a nanocomposite polycaprolactone scaffold. *Biotechnol Appl Biochem* 2009;**54:**221-9

16 Tan A, Farhatnia Y, Seifalian AM. Polyhedral oligomeric silsesquioxane poly(carbonate-urea) urethane (POSS-PCU): applications in nanotechnology and regenerative medicine. *Crit Rev Biomed Eng* 2013;**41:**495-513

17 Loh QL, Choong C. Three-dimensional scaffolds for tissue engineering applications: role of porosity and pore size. *Tissue Eng Part B Rev* 2013;**19:**485-502

18 Hamilton N, Bullock AJ, Macneil S, Janes SM, Birchall M. Tissue engineering airway mucosa: a systematic review. *Laryngoscope* 2014;**124:**961-8

19 Chawla R, Tan A, Ahmed M, Crowley C, Moiemen NS, Cui Z, et al. A polyhedral oligomeric silsesquioxane-based bilayered dermal scaffold seeded with adipose tissue-derived stem cells: in vitro assessment of biomechanical properties. *J Surg Res* 2014;**188:**361-72

20 Nayyer L, Jell G, Esmaeili A, Birchall M, Seifalian AM. A Biodesigned Nanocomposite Biomaterial for Auricular Cartilage Reconstruction. *Adv Healthc Mater* 2016;**5:**1203-12

21 Davis JR. *Tensile Testing*: ASM International; Russell Township, 2004

22 Schindelin J, Rueden CT, Hiner MC, Eliceiri KW. The ImageJ ecosystem: An open platform for biomedical image analysis. *Mol Reprod Dev* 2015;**82:**518-29

23 Butler CR, Hynds RE, Gowers KHC, Lee DDH, Brown JM, Crowley C, et al. Rapid Expansion of Human Epithelial Stem Cells Suitable for Airway Tissue Engineering. *Am J Respir Crit Care Med* 2016;**194**

24 Divieto C, Sassi MP. A first approach to evaluate the cell dose in highly porous scaffolds by using a nondestructive metabolic method. *Future Science OA* 2015;**1**

25 Nayyer L, Birchall M, Seifalian AM, Jell G. Design and development of nanocomposite scaffolds for auricular reconstruction. *Nanomedicine* 2014;**10:**235-46

26 Horst M, Madduri S, Milleret V, Sulser T, Gobet R, Eberli D. A bilayered hybrid microfibrous PLGA–Acellular matrix scaffold for hollow organ tissue engineering. *Biomaterials* 2013;**34:**1537-45

27 Crowley C, Klanrit P, Butler CR, Varanou A, Plate M, Hynds RE, et al. Surface modification of a POSS-nanocomposite material to enhance cellular integration of a synthetic bioscaffold. *Biomaterials* 2016;**83:**283-93

28 Murphy CM, O'Brien FJ. Understanding the effect of mean pore size on cell activity in collagen-glycosaminoglycan scaffolds. *Cell Adh Migr* 2010;**4:**377-81
29 de Mel A, Punshon G, Ramesh B, Sarkar S, Darbyshire A, Hamilton G, et al. In situ endothelialization potential of a biofunctionalised nanocomposite biomaterial-based small diameter bypass graft. *Biomed Mater Eng* 2009;**19:**317-31
30 Freyman TM, Yannas IV, Gibson LJ. Cellular materials as porous scaffolds for tissue engineering. *Progress in Materials Science* 2001;**46:**273-82
31 Liebschner MAK. *Computer-Aided Tissue Engineering*: Humana Press; New York City, 2012
32 Hendow EK, Guhmann P, Wright B, Sofokleous P, Parmar N, Day RM. Biomaterials for hollow organ tissue engineering. *Fibrogenesis & Tissue Repair* 2016;**9:**3
33 Murphy CM, Haugh MG, O'Brien FJ. The effect of mean pore size on cell attachment, proliferation and migration in collagen–glycosaminoglycan scaffolds for bone tissue engineering. *Biomaterials* 2009;**31:**461-6
34 Grayson WL, Bhumiratana S, Cannizzaro C, Chao PH, Lennon DP, Caplan AI, et al. Effects of initial seeding density and fluid perfusion rate on formation of tissue-engineered bone. *Tissue Eng Part A* 2008;**14:**1809-20
35 O'Brien J, Wilson I, Orton T, Pognan F. Investigation of the Alamar Blue (resazurin) fluorescent dye for the assessment of mammalian cell cytotoxicity. *Eur J Biochem* 2000;**267:**5421-6
36 Guo S, DiPietro LA. Factors Affecting Wound Healing. *J Dent Res* 2010;**89:**219-29
37 Pastar I, Stojadinovic O, Yin NC, Ramirez H, Nusbaum AG, Sawaya A, et al. Epithelialization in Wound Healing: A Comprehensive Review. *Adv Wound Care* 2014;**3:**445-64
38 Coraux C, Nawrocki-Raby B, Hinnrasky J, Kileztky C, Gaillard D, Dani C, et al. Embryonic Stem Cells Generate Airway Epithelial Tissue. *Am J Respir Cell Mol Biol* 2005;**32:**87-92
39 Vrana NE, Lavalle P, Dokmeci MR, Dehghani F, Ghaemmaghami AM, Khademhosseini A. Engineering Functional Epithelium for Regenerative Medicine and In Vitro Organ Models: A Review. *Tissue Engineering Part B, Reviews* 2013;**19:**529-43
40 Lutolf MP, Hubbell JA. Synthetic biomaterials as instructive extracellular microenvironments for morphogenesis in tissue engineering. *Nat Biotechnol* 2005;**23:**47-55
41 Anzlovar A, Kogej K, Orel ZC, Zigon M. Polyol mediated nano size zinc oxide and nanocomposites with poly(methyl methacrylate). *Express Polymer Letters* 2011;**5:**604-19
42 Ma Z, Kotaki M Fau - Inai R, Inai R Fau - Ramakrishna S, Ramakrishna S. Potential of nanofiber matrix as tissue-engineering scaffolds. *Tissue Eng* 2005;**11:**101-9
43 Karageorgiou V, Kaplan D. Porosity of 3D biomaterial scaffolds and osteogenesis. *Biomaterials* 2005;**26:**5474-91
44 Q. Chen, J. A. Roether and A. R. Boccaccini, Tissue Engineering Scaffolds from Bioactive Glass and Composite Materials, Chapter 6 in: Topics in Tissue Engineering, Vol. 4. Eds. N Ashammakhi, R Reis, & F Chiellini, 2008.
45 Engler AJ, Sen S, Sweeney HL, Discher DE. Matrix elasticity directs stem cell lineage specification. *Cell* 2006;**126:**677-89
46 Baiguera S, Gonfiotti A, Jaus M, Comin CE, Paglierani M, Del Gaudio C, et al. Development of bioengineered human larynx. *Biomaterials* 2011;**32:**4433-42
47 Asawa Y, Sakamoto T, Komura M, Watanabe M, Nishizawa S, Takazawa Y, et al. Early Stage Foreign Body Reaction against Biodegradable Polymer Scaffolds Affects Tissue Regeneration during the Autologous Transplantation of Tissue-Engineered Cartilage in the Canine Model. *Cell Transplant* 2012;**21:**1431-42
48 Maughan EF, Butler CR, Crowley C, Teoh GZ, Hondt MD, Hamilton NJ, et al. A comparison of tracheal scaffold strategies for pediatric transplantation in a rabbit model. *The Laryngoscope* 2017;**127:**E449-E57

**Summary Sheet**

- Polymeric POSS-PCU has previously shown promise as a tissue engineering scaffold.
- The production of the POSS-PCU foam elastomer involves a stage of phase-separation which results in the formation of a non-porous membrane on its surface. This occurs on contact between de-ionised water and the polymer.
- This study investigated methods for perforating the POSS-PCU surface to allow cell ingress for tissue engineering airways.
- The polymer surface was successfully perforated and imaged using various techniques and preliminary data showed cell attachment, as well as migration, into the scaffold.
- Maintaining a balance between mechanical efficiency, whilst creating a microenvironment that encourages cell migration, is key to the success of the clinical application of POSS-PCU as a laryngeal scaffold.